Machining Science and Technology
Publication details, including instructions for authors and subscription information:
http://www.informaworld.com/smpp/title~content=t713597283

A FORCE PREDICTION MODEL FOR CUTTING UNIDIRECTIONAL FIBRE-REINFORCED PLASTICS

L. C. Zhang[a]; H. J. Zhang[a]; X. M. Wang[a]
[a] The University of Sydney School of Aerospace, NSW, Australia

Online publication date: 30 November 2001

To cite this Article Zhang, L. C. , Zhang, H. J. and Wang, X. M.(2001) 'A FORCE PREDICTION MODEL FOR CUTTING UNIDIRECTIONAL FIBRE-REINFORCED PLASTICS', Machining Science and Technology, 5: 3, 293 — 305
To link to this Article: DOI: 10.1081/MST-100108616
URL: http://dx.doi.org/10.1081/MST-100108616

MACHINING SCIENCE AND TECHNOLOGY, 5(3), 293–305 (2001)

A FORCE PREDICTION MODEL FOR CUTTING UNIDIRECTIONAL FIBRE-REINFORCED PLASTICS

L. C. Zhang,* H. J. Zhang, and X. M. Wang

School of Aerospace, Mechanical and Mechatronic Engineering,
The University of Sydney, NSW 2006, Australia

ABSTRACT

This paper aims to develop an approximate mechanics model to predict the forces in the orthogonal cutting of unidirectional fibre-reinforced plastics when the fibre-orientation varies from 0° to 90°. Based on the experimental understanding achieved, the model divides the cutting zone into three characteristic regions, *i.e*., chipping, pressing and bouncing regions. The cutting tool geometry, such as the rake angle and nose radius, is considered. It shows that the model developed has captured the major deformation mechanisms in cutting the composites and can predict the cutting forces with acceptable accuracy.

1. INTRODUCTION

Fibre-reinforced plastics (FRPs) are an important class of materials in advanced structural applications due to their light weight, high modulus and specific strength. However, because of the anisotropic and heterogeneous nature of the materials, it has been difficult to predict the cutting forces reliably. There have been many studies in the machining of FRPs. For example, Wang and Zhang [1] investigated the cutting of carbon fibre-reinforced composites and found that the machinability and surface integrity are mainly controlled by fibre-orientation. König, *et al.*, [2] reviewed some problems in machining FRPs and Zhang, *et al.*,

* Corresponding author.

[3] discussed the assessment of the exit defects in drilling FRPs and offered some empirical formulae for predicting the spalling size in drilling. Wang, Ramulu and Arola [4] studied the effect of tool geometry and fibre-orientation and Bhatnagar, *et al.* [5] used a shear test to evaluate the in-plane shear strength of FRP specimens and proposed a model for cutting force prediction. Arola and Ramulu [6] and Mahdi and Zhang [7] applied the finite element method to investigate the cutting of FRPs but the former adopted a homogenized material model and the latter considered the micro details of individual fibre-tool interactions. Puw and Hocheng [8] summarized some cutting mechanisms and reviewed a mathematical force prediction model for milling.

In short, the investigations on cutting FRPs can be generally divided into three categories: (1) experimental study focusing on macro/microscopic behavior of FRPs, (2) simple modelling using conventional metal cutting mechanics, and (3) numerical simulations that treat the FRPs as macroscopically anisotropic materials or concentrate on the fibre-matrix interactions microscopically. Nevertheless, the existing macroscopic models ignored many fundamental characteristics of FRPs subjected to cutting and did not integrate well with the true cutting mechanics, while those focusing on the micro-effects were unable to offer a formula for practical use.

This paper tends to develop an approximate mechanics model to predict the forces in cutting composites reinforced by unidirectional fibres. The understanding of the cutting mechanisms in the modeling was achieved by experimental observations.

2. MAJOR EXPERIMENTAL FINDINGS

A surface grinder, MININI M286, was modified for the orthogonal cutting experiment, with the grinding wheel being replaced by a cutting tool. The hydraulic table of the machine, on which an FRP specimen was held, provided a steady cutting motion. The cutting forces were measured by a three-dimensional dynamometer, Kistler 9257B, which was attached to the hydraulic table. The cutting speed was fixed at 1m/min. Two commercial resin systems, the F593 and MTM56 prepregs, were used to make unidirectional carbon/epoxy panels with the desired fibre-orientation for the cutting experiment. The fibre-orientation, θ, is defined clockwise with respect to the cutting direction, as shown in Fig. 1. The cutting tools used were made from tungsten carbide with a clearance angle of 7° and rake angles from $-20°$ to 40°. Table 1 lists the cutting conditions used.

It was found that the fibre-orientation is a key factor that determines the surface integrity of a machined component, as shown in Fig. 2. $\theta = 90°$ is a critical angle, beyond which severe subsurface damages will occur, surface roughness will increase remarkably and the deformation mechanisms in the cutting zone will change.

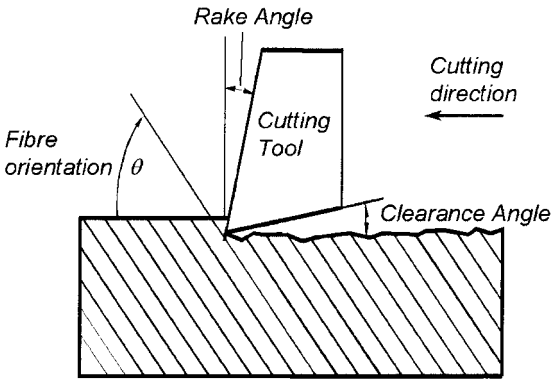

Figure 1. A schematic of the orthogonal cutting of an FRP with unidirectional fibres orientated between 0° and 90°.

It was observed that there exist three distinct deformation regions in the cutting zone, as denoted in Fig. 3, when the fibre-orientation, θ, varies between 0° and 90°. The first region is in front of the rake face, resulting in a chip, called a *Chipping Region* or *Region 1*. Fracture occurs at the cross-sections of the fibres and along the fibre-matrix interfaces. The chipping along an overall shear plane, as shown in the figure, is the result of a zigzag cracking of the fibres perpendicular to the fibre axes and the fibre-matrix interface debonding in the fibre-axis direction. The second distinct deformation region takes place under the nose of the cutting tool, where the nose pushes down the workpiece material. For convenience, it is called the *Pressing Region* or *Region 2*. The third region, called the *Bouncing Region* or *Region 3*, involves mainly the bouncing back of the workpiece material, which happens under the clearance face of the cutting tool.

When the fibre-orientation is beyond 90°, more deformation mechanisms take place. As illustrated in Fig. 4, both the fibre-matrix debonding and fibre bending contribute significantly to the deformation and material removal. Because of the debonding, the depth of the subsurface damage becomes much greater, as shown in Fig. 2(b). The bending of the fibres makes the breakage point of a fibre vary with the movement of the cutting tool and as demonstrated in Fig. 2, the quality of a machined surface gets much poorer.

Table 1. Machining Conditions

	MTM56 Specimens	F593 Specimens
Fibre-orientation (°)	0, 30, 60, 90, 120, 150	0, 30, 60, 90, 120, 150
Rake angle (°)	0	−20, 0, 20, 40
Depth of cut (mm)	0.025, 0.050, 0.075, 0.100, 0.125, 0.150, 0.175, 0.200, 0.250	0.001, 0.050, 0.100

MARCEL DEKKER, INC.
270 Madison Avenue, New York, New York 10016

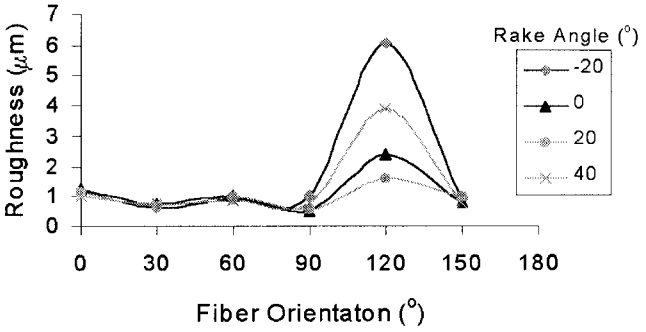

(a)

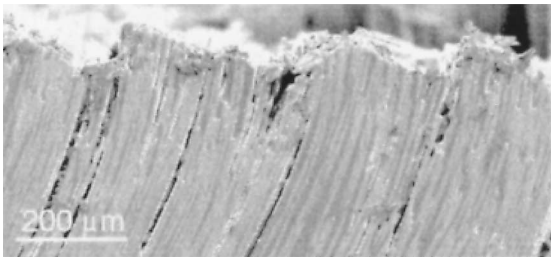

(b)

Figure 2. Effect of fibre-orientation (F593 panels) (a) surface roughness (depths of cut = 0.001mm), (b) Microstructure in the subsurface (fibre-orientation = 120°, depth of cut = 0.100mm, rake angle = 0°).

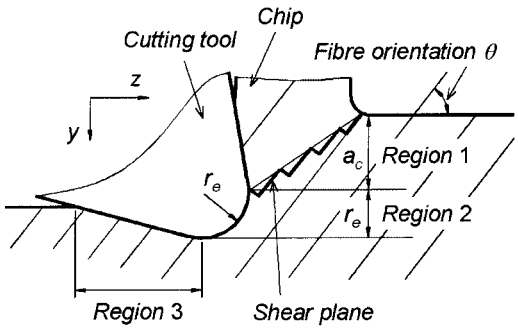

Figure 3. Definitions of the cutting variables and deformation zones when the fibre-orientation is smaller than 90°.

MARCEL DEKKER, INC.
270 Madison Avenue, New York, New York 10016

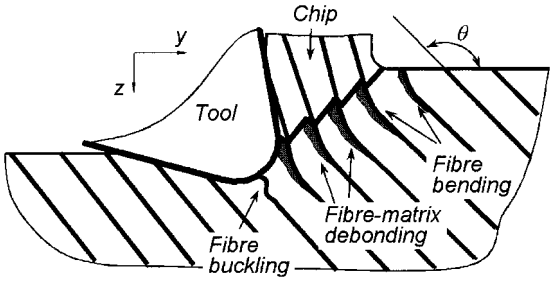

Figure 4. Fibre-bending and fibre-matrix debonding during cutting when the fibre-orientation is larger than 90°.

3. MODELLING

Based on the above understanding, the mechanics modeling of cutting needs to be conducted differently when $\theta \leq 90°$ or when $\theta > 90°$. This study will focus on the case with $\theta \leq 90°$. The modeling with $\theta > 90°$ will be discussed in a separate paper.

The deformation mechanisms demonstrated in Fig. 3 suggests that the cutting zone in mechanics modeling should be also divided into three distinct regions. Region 1 has a depth of a_c, as illustrated in Figs. 2 and 5, bounded by the starting point of the tool nose according to the experiment. Region 2 covers the whole domain under the tool nose, as indicated in Fig. 6, having a depth equal to the nose radius, r_e. Region 3 starts from the lowest point of the tool, as shown in Fig. 7. We assume that the total cutting force can be calculated by adding up the forces in all the three regions, *i.e.*, we assume that the principle of superposition applies. For convenience, the positive directions of the forces are taken to be in the positive y- and z-directions as defined in Fig. 3.

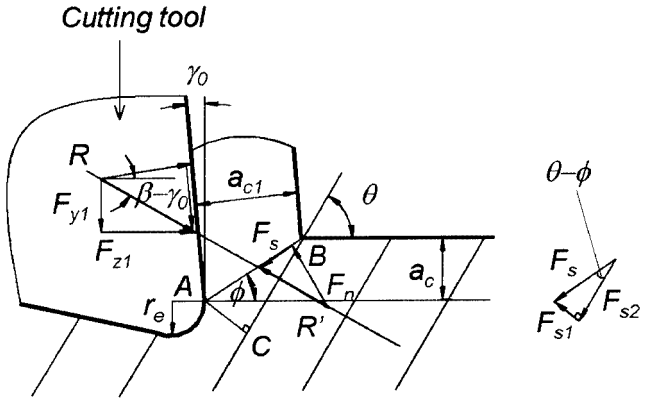

Figure 5. The cutting force diagram in Region 1.

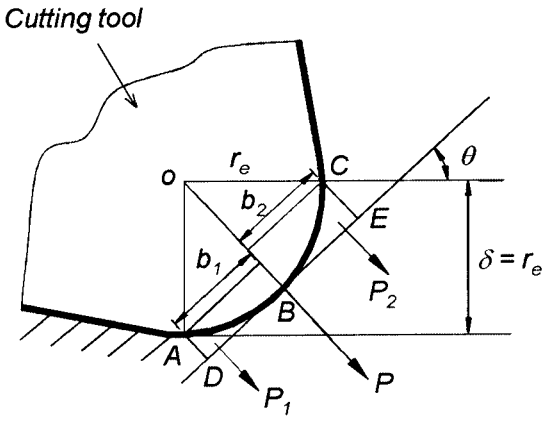

Figure 6. The contact between the tool nose and the workpiece material in Region 2.

3.1 Region 1—Chipping

Chipping occurs in this region and the process is similar to a normal orthogonal cutting with a sharp cutting tool. Figure 5 shows its cutting force diagram, where *AB* is a theoretical shear plane, formed by many micro events of the cross-section fracture of fibres, along *AC*, and fibre-matrix debonding, along *CB*, as described in the last section.

In this region, the resultant force R is equal and opposite to the resultant force R' which consists of a shear force and a normal force acting on the shear plane *AB*. The shear force can be further resolved into Fs_1, which cuts the fibres along *CA*, and Fs_2, which cuts the matrix or delaminates the fibre-matrix interface along *BC*, parallel to the fibre axis. Clearly, Fs_1 and Fs_2 can be written as

$$\begin{cases} F_{s1} = F_s \cdot \sin(\theta - \phi) \\ F_{s2} = F_s \cdot \cos(\theta - \phi) \end{cases} \tag{1}$$

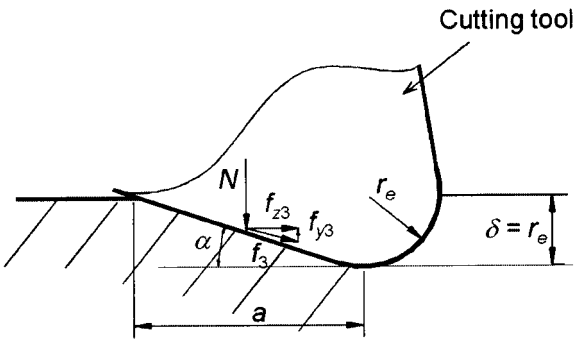

Figure 7. The contact in Region 3.

MARCEL DEKKER, INC.
270 Madison Avenue, New York, New York 10016

where θ is the fibre-orientation varying from 0° to 90° and ϕ is the shear plane angle to be determined. On the other hand, if τ_1 and τ_2 are the shear strengths of the work material in *AC* and *BC* directions, respectively, the two shear forces can be expressed as

$$\begin{cases} F_{s1} = \tau_1 \cdot l_{AC} \cdot h \\ F_{s2} = \tau_2 \cdot l_{BC} \cdot h \end{cases} \tag{2}$$

where l_{AC} is the total length of all the cross section fractures along *AC*, l_{BC} is the total length of all the matrix fractures along *BC* and *h* is the thickness of the workpiece material perpendicular to the *yz*-plane. Therefore, by equating Eqs. (1) and (2), we obtain

$$\frac{l_{BC}}{l_{AC}} = \frac{\tau_1}{\tau_2 \cdot \tan(\theta - \phi).} \tag{3}$$

According to Fig. 5, we also have

$$l_{BC} \cdot \sin\theta - l_{AC} \cdot \cos\theta = a_c, \tag{4}$$

where a_c is the real depth of cut. Equations (3) and (4) then give rise to

$$l_{AC} = \frac{a_c}{\dfrac{\tau_1 \cdot \sin\theta}{\tau_2 \cdot \tan(\theta - \phi)} - \cos\theta}. \tag{5}$$

Therefore, using Eqs. (1), (2) and (5), the total shear force F_s in Region 1 can be calculated by

$$F_s = \frac{\tau_1 \cdot h \cdot a_c}{\dfrac{\tau_1}{\tau_2} \cdot \cos(\theta - \phi) \cdot \sin\theta - \sin(\theta - \phi) \cdot \cos\theta}. \tag{6}$$

Since

$$F_n = F_s \cdot \tan(\phi + \beta - \gamma_o), \tag{7}$$

where β is the friction angle on the rake face, referring to Fig. 5 again, we have

$$\begin{pmatrix} F_{z1} \\ F_{y1} \end{pmatrix} = \begin{pmatrix} \sin\phi\cos\phi \\ \cos\phi - \sin\phi \end{pmatrix} \begin{pmatrix} F_n \\ F_s \end{pmatrix}, \tag{8}$$

where F_{y1} and F_{z1} are vertical and horizontal cutting forces. Hence the substitution of Eqs. (6) and (7) into Eq. (8) yields the cutting forces in Region 1:

$$\begin{cases} F_{z1} = \tau_1 \cdot h \cdot a_c \cdot \dfrac{\sin\tau \cdot \tan(\phi + \beta\,\gamma_o) + \cos\phi}{\dfrac{\tau_1}{\tau_2} \cdot \cos(\theta - \phi) \cdot \sin\theta - \sin(\theta - \phi) \cdot \cos\theta} \\ F_{y1} = \tau_1 \cdot h \cdot a_c \cdot \dfrac{\cos\phi \cdot \tan(\phi + \beta - \gamma_o) - \sin\phi}{\dfrac{\tau_1}{\tau_2} \cdot \cos(\theta - \phi) \cdot \sin\theta - \sin(\theta - \phi) \cdot \cos\theta} \end{cases} \tag{9}$$

To calculate the forces using Eq. (9), ϕ needs to be determined. According to the general cutting mechanics, we have

$$\tan\phi = \frac{r_c \cdot \cos\gamma_o}{1 - r_c \cdot \sin\gamma_o}$$

where γ_o is the rake angle of the tool and

$$r_c = \frac{a_c}{a_{c1}}$$

in which a_{c1} is the chip thickness. Because an FRP in cutting behaves like a typical brittle material [1], it is reasonable to let $r_c = 1$. Therefore,

$$\phi \approx \tan^{-1}\left(\frac{\cos\gamma_0}{1 - \sin\gamma_0}\right).$$

3.2 Region 2—Pressing

The deformation in Region 2 is caused by the tool nose, which can be viewed as the deformation under a cylindrical indenter, as shown in Fig. 6. Since *DB* and *BE* are generally unequal when the fibre-orientation, θ, varies, the tool nose indentation by surfaces *AB* and *BC* needs to be considered separately. Again, we assume that the principle of superposition applies. By using the indentation mechanics of a circular cylinder in contact with a half-space [9], the indentation force on the tool nose can be approximately calculated by adding up half of the indentation forces on arc lengths 2*AB* and 2*BC*. We therefore obtain

$$\begin{cases} P_1 = \dfrac{1}{2} \cdot \dfrac{b_1^2 \cdot \pi \cdot E^* \cdot h}{4 \cdot r_e}, \\ P_2 = \dfrac{1}{2} \cdot \dfrac{b_2^2 \cdot \pi \cdot E^* \cdot h}{4 \cdot r_e}, \end{cases} \tag{10}$$

where P_1 and P_2 are the indentation forces, perpendicular to the fibre axis, that the tool nose exerts on *AB* and *BC*, respectively. E^* is the effective elastic modulus of the workpiece material in the direction of P_1 and P_2, h is the thickness of the workpiece, r_e is the nose radius and b_1 and b_2 are the widths of the contact arcs *AB* and *BC*, which can be calculated as

$$\begin{cases} b_1 = r_e \cdot \sin\theta \\ b_2 = r_e \cdot \cos\theta \end{cases} \tag{11}$$

The effective elastic modulus E^* is defined by

$$E^* = \frac{E}{1 - \nu^2}, \tag{12}$$

where E is the Young's modulus of the workpiece material in the direction of OP in Fig.6, and ν is the minor Poisson's ratio. The resultant force P is therefore

$$P = P_1 + P_2. \tag{13}$$

It must be pointed out that Eq. (10) is based on the contact mechanics of elastic deformation. In a cutting, however, the deformation of the workpiece material under the pressing of the tool nose must have introduced micro-cracking and failure of matrix. To take such micro-effects into account, the resultant force P can be approximately modified by

$$P_{real} = K \cdot P, \tag{14}$$

where P_{real} is called the real resultant force in Region 2 in which the coefficient K is a function of fibre-orientation, *i.e.*, $K = f(\theta)$, to be determined by experiment. Combining Eqs. (10) to (14), we get

$$\begin{cases} F_{y2p} = P_{real} \cdot \cos\theta \\ F_{z2p} = P_{real} \cdot \sin\theta \end{cases}$$

When the friction coefficient is μ, the frictional force

$$f_{real} = P_{real} \cdot \mu,$$

can be resolved as

$$\begin{cases} f_{y2} = P_{real} \cdot \mu \cdot \sin\theta \\ f_{z2} = P_{real} \cdot \mu \cdot \cos\theta \end{cases}$$

Finally, the total cutting forces in Region 2 become

$$\begin{cases} F_{y2} = P_{real} \cdot (\cos\theta - \mu \cdot \sin\theta) \\ F_{z2} = P_{real} \cdot (\sin\theta + \mu \cdot \cos\phi) \end{cases} \tag{15}$$

3.3 Region 3—Bouncing

In this region, the contact force between the clearance face and the workpiece material is caused by the bouncing back of the workpiece material.

For simplicity, assume that the bouncing back is complete, *i.e.*, the height of the bouncing back is equal to the thickness of Region 2, r_e. Thus the contact length, a, in Region 3, as illustrated in Fig.7, can be obtained as

$$a = \frac{r_e}{\tan \alpha} \tag{16}$$

where α is the clearance angle of the tool. Using the contact mechanics between a wedge and a half-space [10], the total force N can be calculated by

$$N = \frac{1}{2} \cdot a \cdot E_3 \cdot \tan \alpha \cdot h, \tag{17}$$

where E_3 is the effective modulus of the workpiece material in Region 3, which must be smaller than that of the original workpiece material, because the material in this region has been damaged during the deformation experienced in Region 2 and thus has become weaker. Using Eq.(16), we get

$$N = \frac{1}{2} \cdot r_e \cdot E_3 \cdot h.$$

The friction force f_3 between the clearance face of the cutting tool and the workpiece material is μN and can also be resolved into y- and z-directions to get f_{y3} and f_{z3}. Hence, the cutting forces in Region 3 are

$$\begin{cases} F_{y3} = \dfrac{1}{2} \cdot r_e \cdot E_3 \cdot h \cdot (1 - \mu \cdot \cos \alpha \cdot \sin \alpha) \\ F_{z3} = \dfrac{1}{2} \cdot r_e \cdot E_3 \cdot h \cdot \cos^2 \alpha \end{cases} \tag{18}$$

3.4 The Total Cutting Forces

The total forces, F_z and F_y, are the summation of the corresponding components from the above three regions, *i.e.*,

$$\begin{cases} F_y = F_{y1} + F_{y2} + F_{y3} \\ F_z = F_{z1} + F_{z2} + F_{z3} \end{cases} \tag{19}$$

where F_{yi} and F_{zi} ($i = 1, 2, 3$) are defined in Eqs. (9), (15) and (18), respectively. In this mechanics model, the parameters to be determined by experiment, when a workpiece material is given, are τ_1, τ_2, β, E, ν, μ, E_3 and K.

4. COMPARISON WITH EXPERIMENT

We focus on two materials, MTM56 and F593 [1], of which the property parameters and results in terms of cutting forces were experimentally available for examining the validity of the model. With these materials, it was found that $\tau_1 = 90$MPa, $\tau_2 = 20$MPa, $\beta = 30°$, $\mu = 0.15$, $E = 10$GPa, $\nu = 0.026$ and

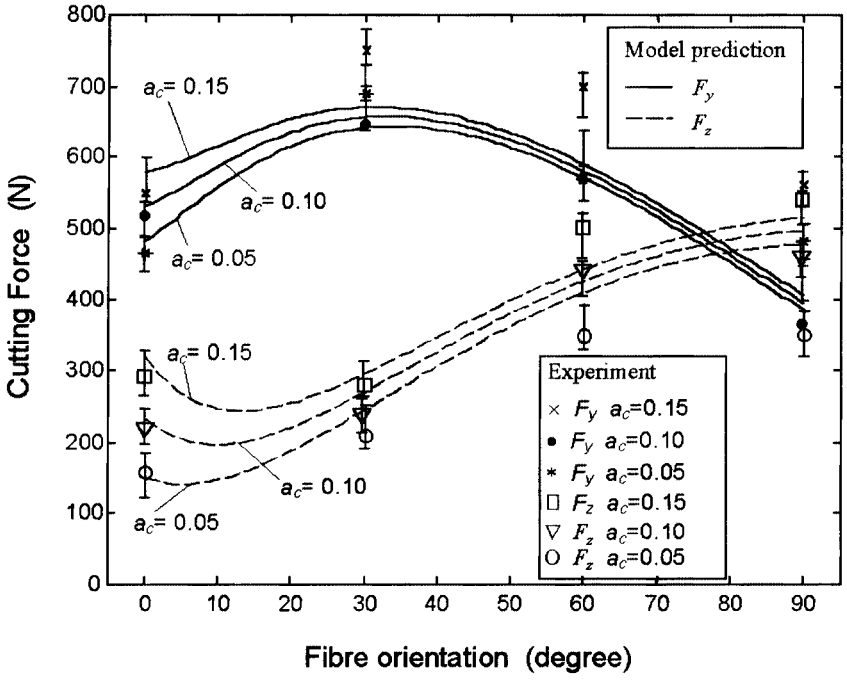

Figure 8. Comparison between model predictions and experimental measurements when the depth of cut and fibre-orientation change (Material: MTM56, $E_3 = 5.5$GPa).

$K = 0.5 \cdot \tan^{-1}(30/\theta)$. For MTM56, the effective modulus in Region 3 is $E_3 = 5.5$GPa, while that for F593 is $E_3 = 3.5$GPa. The specimen thickness is $h = 4$mm.

Figures 8 and 9 show the comparison between the model predictions and experimental measurements [1]. It can be seen that although the model involves simplifications and assumptions as presented in the previous section, it predicts nicely the nature of the cutting force variation when the cutting parameters change, such as the depth of cut, fibre-orientation and rake angle. This means that the model has captured the major deformation mechanisms in cutting the FRPs. However, the maximum error in predicting the vertical force is 37% and that in predicting the horizontal force is 27%. The errors are relatively large but it is understandable because experimental measurements were influenced by many factors in manufacturing the FRP specimens, for instance, the inability to align the fibres perfectly in a desired uni-direction or to distribute them uniformly throughout a specimen.

5. CONCLUSION

This paper developed an analytical mechanics model for predicting the forces in cutting the FRPs of fibre-orientation varying from 0° to 90°. A comparison with

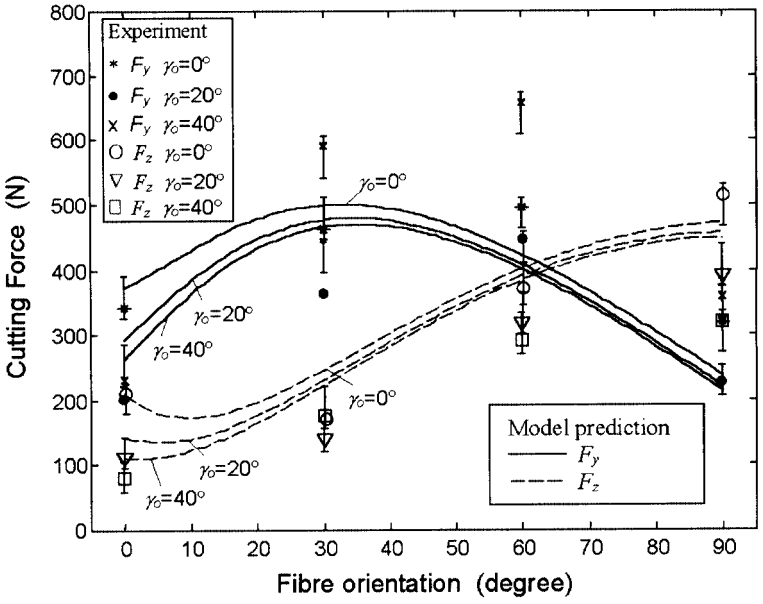

Figure 9. Comparison between model predictions and experimental measurements when the rake angle and fibre-orientation change (Material: F593, E_3 = 3.5GPa).

experiment shows that the model, though approximate, has captured the major deformation mechanisms in the cutting zone.

When the fibre-orientation is greater than 90°, a cutting involves some other deformation mechanisms. The modelling with $90° < \theta < 180°$ is currently undertaking in the authors' research laboratory.

ACKNOWLEDGEMENT

The research was sponsored by an ARC Large Grant.

REFERENCES

1. X. Wang and L. Zhang, ''Machining Damage in Unidirectional Fibre-Reinforced Plastics,'' in: Abrasive Technology—Current Development and Applications, edited by J Wang, W Scott and L Zhang, World Scientific, Singapore (1999) pp. 429–436.
2. W. König, Ch. Wulf, P. Graß and H. Willerscheid, ''Machining of Fibre Reinforced Plastics,'' Annals of the CIRP, 34(2) (1985) 537–548.
3. H. Zhang, W. Chen, D. Chen and L. Zhang, ''Assessment of the Exit Defects in Carbon Fibre-Reinforced Plastic Plates Caused by Drilling,'' Key Engineering Materials, 196 (2001) 43–52.
4. D. H. Wang, M. Ramulu and D. Arola, ''Orthogonal Cutting Mechanisms of

Graphite/Epoxy Composite, Part I: Unidirectional Laminate,'' International Journal of Machine Tools and Manufacture, 35 (1995) 1623–1638.
5. N. Bhatnagar, N. Ramakrishnan, N. K. Naik and R. Komanduri, ''On the Machining of Fiber Reinforced Plastic (FRP) Composite Laminates,'' International Journal of Machine Tools and Manufacture, 35 (1995) 701–716.
6. D. Arola and M. Ramulu, ''Orthogonal cutting of Fiber-Reinforced Composites: A Finite Element Analysis,'' International Journal of Mechanical Science, 39 (1997) 597–613.
7. M. Mahdi and L. Zhang, ''A Finite Element Model for the Orthogonal Cutting of Fibre-Reinforced Composite Materials,'' Journal of Materials Processing Technology, 113 (2001) 373–377.
8. H. Y. Puw and H. Hocheng, ''Milling of Polymer Composites,'' in: Machining of Ceramics and Composites, edited by S. Jahanmir, M. Ramulu and P. Koshy, Marcel Dekker Inc., New York (1999) pp. 267–294.
9. L. Zhang, Solid Mechanics for Engineers, Macmillan Press, Basingstoke, UK (2001).
10. K. L. Johnson, Contact Mechanics, Cambridge University Press, Cambridge, UK (1985).

MARCEL DEKKER, INC.
270 Madison Avenue, New York, New York 10016

Request Permission or Order Reprints Instantly!